PROCEEDINGS OF SCIENCE

The second knee in the cosmic ray spectrum observed with the surface detector of the Pierre Auger Observatory

Gabriel Brichetto Orquera[a,b,*] **for the Pierre Auger Collaboration**[c]

[a] *Instituto de Tecnologías en Detección y Astropartículas (CNEA, CONICET, UNSAM), Av. General Paz 1555 (B1630KNA) San Martín, Buenos Aires, Argentina,*

[b] *Institute for Astroparticle Physics (IAP), Karlsruhe Institute of Technology, P.O. Box 3640, 76021 Karlsruhe, Germany*

[c] *Observatorio Pierre Auger, Av. San Martín Norte 304, 5613 Malargüe, Argentina*

Full author list: https://www.auger.org/archive/authors_icrc_2023.html

E-mail: spokespersons@auger.org

The determination of the energy spectrum features with low systematic uncertainty is crucial for interpreting the nature of cosmic rays. In this study, we conducted a measurement of the energy spectrum at the Pierre Auger Observatory using a surface detector with a calorimetric energy scale indirectly set by a fluorescence detector. The surface detector consists of an array of water-Cherenkov detectors that extends over 3000 km^2 with 1500 m spacing. Additionally, two nested arrays of the same kind with 750 m and 433 m spacing were utilized to lower the energy threshold of the measurements. This contribution presents, for the first time, the spectrum measured with the 433 m array, which reduces the energy threshold down to 63 PeV, nearly half the energy at which we previously published a steepening using the 750 m array. Our measurements include a characterization of the spectral features of the flux steepening around 230 PeV, known as the second-knee. The study benefits from a nearly 100% duty cycle and geometrical exposure. Notably, this is the first simultaneous measurement of the second knee energy and spectral indexes before and after the break, using a surface detector with an energy scale predominantly independent of air shower simulations and assumptions regarding hadronic interaction models.

38th International Cosmic Ray Conference (ICRC2023)
26 July – 3 August, 2023
Nagoya, Japan

*Speaker

PoS(ICRC2023)398

1. Introduction

The concept that the Galactic-to-extragalactic transition occurs between 100 PeV and a few EeV is well-accredited [1–5]. It is thus to be expected that different astrophysical phenomena are at play in this energy region, that overlap and intertwine with each other. To disentangle them, a precise measurement of the all-particle energy spectrum and of the abundance of the different elements as a function of energy is crucial. It is for this purpose that the Pierre Auger collaboration has built two denser surface arrays, spaced at 750 m (SD750) and at 433 m (SD433) nested in the one spaced at 1500 m (SD1500), for a high statistics measurement of the spectrum in this region. Also, it is enriching them, in the context of the Observatory upgrade, with muon detectors that will allow inferring the mass of cosmic rays [6] and searching for primary photons [7]. Using data from SD750 we measured the energy spectrum down to 100 PeV, at which we observed a broad softening [8]. Here we report for the first time the measurement of the energy spectrum made with the SD433, capable of reaching down to 63 PeV, thus enabling a comprehensive characterization of the second knee. The SD433, which consists of an array of 19 water-Cherenkov detectors (WCD) identical to those used in the other two Auger surface arrays [9] and is nested within the SD750 with which it shares seven detectors, is depicted in Fig. 1. Data collection with the SD433 began in 2013 with a hexagon of WCDs installed surrounding a central detector. Over time the SD433 was expanded and reached its current configuration in May 2019. The data acquisition period concluded with the replacement of the detector electronics as part of the upgrade. In Section 2 we provide the details of the SD433 response obtained from simulations. Section 3 focuses on the energy calibration of the SD433 followed by Section 4 where we present the measurement of the spectrum, based on data collected from 28 January 2018 to 21 December 2021.

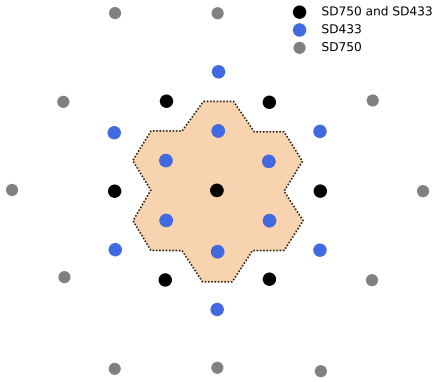

Figure 1: Map of the SD433. The array consists of 19 water-Cherenkov detectors spaced at 433 m. The effective area is shown in light orange.

2. SD433 energy response

We consider in this section the trigger efficiency, the energy resolution, and the energy bias of the SD433, three of the ingredients required to construct the energy spectrum. We characterized the response of the array with CORSIKA simulations using EPOS-LHC and FLUKA as the high- and low-energy hadronic-interaction models, respectively. We accounted for the effect of the primary-mass composition by running simulations for different primary-mass groups. We took the relative weight of each group from the composition determined by the Global Spline Fit [10]. Afterward, we simulated the SD433 signals and reconstructed the resulting events with the Offline framework [11]. Given the deficiencies in the extrapolation of hadronic models beyond the energies

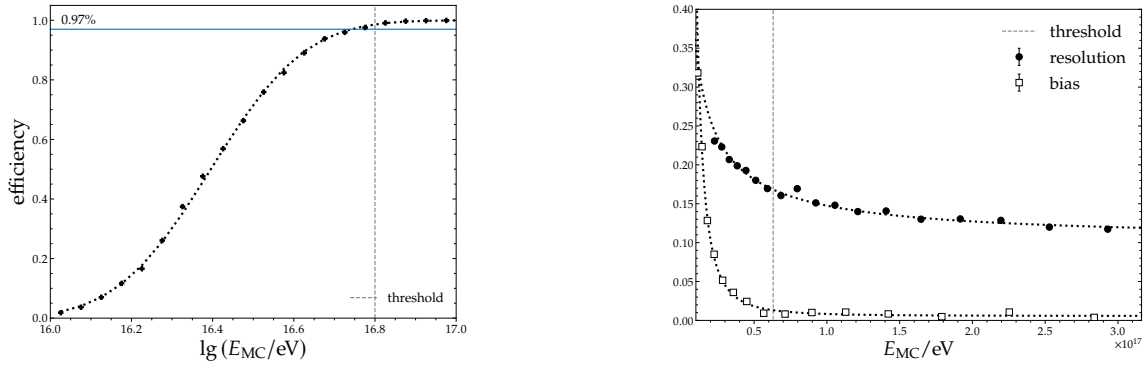

Figure 2: Trigger efficiency (left), energy resolution, and energy bias (right) of the SD433 determined by Monte-Carlo CORSIKA simulations. The full efficiency threshold is indicated by a vertical dashed line.

of the accelerator data, the signal sizes derived from simulations are known to differ from cosmic-ray data. To compensate for this effect we applied separate calibrations for simulations and data.

The efficiency of a surface detector is the probability of a shower triggering it. For a given array geometry, the efficiency is governed by the energy, the zenith angle, and the mass of the primary. In 2014 two new station level triggers were deployed [8]. These triggers were included in the simulation since they are more sensitive to the low-energy electromagnetic component of the shower, thus reducing the threshold energy of the spectrum. Fig. 2 (left) shows the efficiency for events arriving with zenith angle $\theta \leqslant 45^\circ$, as determined by the simulations. We fitted the efficiency with the model [12]

$$\epsilon(E) = \frac{1}{2}\,\mathrm{erf}\left[a\,\lg\left(\frac{E}{10\,\mathrm{PeV}}\right) + b\right] + \frac{1}{2}. \tag{1}$$

The best fit parameters are $a = 3.88 \pm 0.02$ and $b = -1.54 \pm 0.01$. The threshold energy for the spectrum measurement is defined as that at which the efficiency is greater than 97 %: for the SD433 is at $\lg(E/\mathrm{eV}) = 16.8$ ($E = 63\,\mathrm{PeV}$).

We calculated the SD433 resolution as the ratio of the standard deviation of the reconstructed energy to the simulated energy. We binned the energy ratio and calculated its mean as shown in Fig. 2. The resolution improves with the energy and is 17% at the SD433 threshold energy. We fitted the resolution ($\sigma(E)/E$) with a model that adds in quadrature a contribution of the fluctuations in the shower development for different events (R_{sh}) and another term corresponding to the statistical uncertainty in the reconstructed shower size given the sparse sampling of the shower front by the surface detector and the finite size of the WCD,

$$\left(\frac{\sigma(E)}{E}\right)^2 = R_{\mathrm{sh}}^2 + \frac{R_0^2}{E/E_0}. \tag{2}$$

We assumed the shower term to be constant and the detector contribution to scale with the square root of the energy. The parameter R_0 corresponds to the SD433 resolution for a reference energy $E_0 = 100\,\mathrm{PeV}$. By fitting the resolution model to the data, we estimated $R_{\mathrm{sh}} = 0.12$ and $R_0 = 0.09$. The detector resolution is dominant at low energies whereas the shower fluctuations drive the total resolution at high energies.

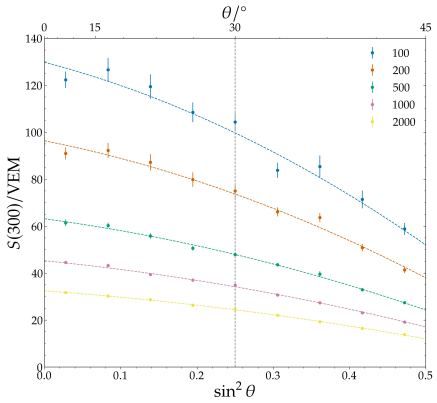

Figure 3: Attenuation of the shower size with the zenith angle for five different intensity cuts. The data and their corresponding fits are shown. The reference angle is indicated by a vertical dashed line.

The reconstructed energy is biased for events with energy below the full-efficiency threshold, because upward fluctuations in the WCD signals make the trigger probability higher, so that larger signals translate into reconstructed ones larger than true ones. To determine the bias, we calculated the difference between the mean of the reconstructed energy and the simulated energy. Fig. 2 shows that the bias decreases with the energy as the array becomes more efficient and is only 2% at the threshold energy. The bias at high energy is close to zero by design as the SD433 is calibrated against the simulated energy.

3. Energy estimation

We reconstructed the SD433 events with the $\overline{\text{Off}}\underline{\text{line}}$ framework using the same method applied for the SD750 and SD1500 arrays. The fall-off of the WCD signal with the distance to the shower axis is fitted with a lateral distribution function modeled as a modified version of the Nishimura-Kamata-Greisen function [12]. We evaluated the fitted lateral distribution function at a reference distance of 300 m to estimate the shower size $S(300)$.

We corrected the shower size to account for its attenuation with the zenith angle using the constant-intensity cut method. This procedure started by classifying the reconstructed shower sizes in nine zenith-angle bins of the same size in $\sin^2\theta$, in the range between 0° to 45°. In each bin, we ordered the events in decreasing $S(300)$ and recorded the values at N = 100, 200, 500, 1000, and 2000 intensities as shown in Fig. 3. We delimited the error intervals with the $S(300)$ at $\pm\sqrt{N}$ away from the cut intensity N. The cornerstone of the constant-intensity cut is that if events arrive isotropically, the $S(300)$ of all bins at a given intensity cut correspond to the same energy. As the isotropy condition requires full efficiency above all cuts, we took that last cut at 2000 events which corresponds to $E \approx 100$ PeV. We modelled the attenuation of $S(300)$ using a second degree polynomial in terms of the variable $x = \sin^2\theta - \sin^2 30°$,

$$S(300) = S_{30}\,[1 + a(S_{30})\,x + b\,x^2], \tag{3}$$

where the factor S_{30} is an energy estimator independent of the zenith angle that can be interpreted as the $S(300)$ the shower has had it arrived at 30°. This reference angle is the median of an isotropic

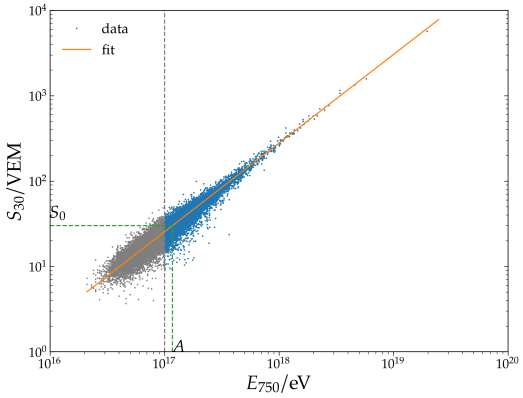

Figure 4: Energy calibration of the SD433 using the events observed in coincidence with the SD750. A selection cut is applied at $E_{750} = 100\,\text{PeV}$, the energy threshold of the SD750. The calibration parameter A and the reference shower size S_0 are displayed.

distribution of arrival directions up to 45°. The attenuation among different cuts is not the same but varies only within less than 3%. We corrected for this small systematic dependence by expanding the linear parameter a so that $a(S_{30}) = a_0 + a_1 \lg(S_{30}/(30\,\text{VEM}))$. We simultaneously fitted the data of all cuts with the model and obtained the parameters $a_0 = 1.66 \pm 0.02$, $a_1 = -0.19 \pm 0.09$, and $b = -1.41 \pm 0.13$ with a $\chi^2 = 34$ for 37 degrees of freedom.

The SD1500 and SD750 are calibrated against the fluorescence detector using events detected in coincidence. For these calibration events, the shower size of the surface detector is correlated with the energy measured by the FD. The advantage of this method is that the fluorescence detector provides an almost calorimetric measurement of the energy. However, it is not possible to apply this approach to the SD433 calibration since, due to its energy range and distance to the nearest telescopes, there are very few coincident events. To overcome this problem we instead correlated the S_{30} of the SD433 with the energy assigned to the same event by the SD750. As the energy scale of the SD750 is set by the FD, the SD433 energies are also inherited from the FD.

We used in the SD433 calibration a set of events that triggered and were reconstructed by both the SD433 and the SD750. We selected events for which the SD750 measures an energy E_{750} greater than 100 PeV, its full efficiency threshold. We also required a zenith angle of less than 45° and that the detector with the highest signal is surrounded by six working detectors in both arrays. After applying these conditions, there are more than 9 700 calibration events. Fig. 4 shows the SD433 calibration. As in the case of the other two surface detectors, a power-law function is used as the calibration model,

$$E = A \left(\frac{S_{30}}{30\,\text{VEM}} \right)^B , \tag{4}$$

where the parameter A corresponds to the energy at $S_{30} = 30$ VEM and the parameter B is the power law index. The model is adjusted to the data by maximizing a likelihood function that considers the combined effect of the energy resolution of both arrays, the shape of the spectrum, and the cut at the threshold energy [13]. In the likelihood, we also included the correlation between S_{30} and E_{750} that is present as both detectors sample the same shower front and also share some WCDs. By

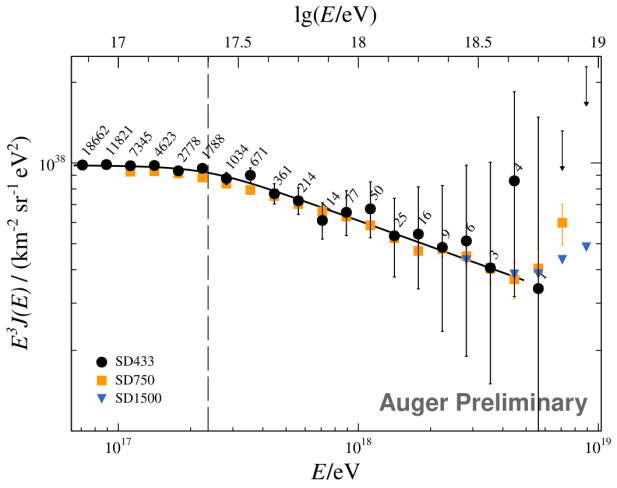

Figure 5: Unfolded cosmic ray spectrum measured with the SD433. The data were fitted with a broken power law model with soft transitions. The position of the fitted second knee is shown in dashed line. The error bars and upper limits correspond to the statistical uncertainty given by the 90% confidence level Feldman-Cousins intervals. The SD750 [8] and SD1500 [15] measurements are also shown.

applying this procedure we estimated the parameters $A = (117.0 \pm 0.4)$ PeV and $B = 0.963 \pm 0.003$ with their correlation $\rho = -0.60$. We used these values of A and B to estimate the energy of each SD433 event from its S_{30} by applying the Eq. (4).

4. Measurement of the spectrum

To ensure an unbiased estimation of the spectrum we selected events in which the WCD with the highest signal is surrounded by six working WCDs. According to this containment condition, the hottest detector of an event has to be one of the seven internal WCDs of the SD433. We also limited the zenith angle of the selected events below 45° as they as they are less attenuated than more inclined events and are dominated by the electromagnetic component [12]. The WCDs trigger upon the fulfillment of any of four different conditions including the two modes implemented at the start of Auger [14] plus two additional modes implemented in 2013. Since the spectrum is measured above an energy at which the SD433 is more than 97% efficient, the exposure can be calculated from the array geometry without resorting to simulations. Considering the aforementioned containment condition, the selected events must fall in the shaded region shown in Fig. 1, which has an area of 1.14 km^2. From the effective area and the maximum zenith angle, the aperture, 1.79 km^2 sr, is obtained when all WCDs are functioning. Given that occasionally some detectors may be down, the instantaneous aperture is less than this nominal value. To measure the aperture of the SD433, the acquisition system records the state of its WCDs every 1 s. The periods in which the data acquisition is unstable are not considered in the computation of the exposure and, correspondingly, the events observed during these periods are excluded from the spectrum. These problems reduced the exposure by only 3%. The resulting exposure of the SD433 is 3.85 km^2 sr yr with a systematic uncertainty of 4%.

To measure precisely the spectrum, the finite energy resolution and the bias of the SD433, which cause the migration of events to neighbouring bins, must be taken into account. We considered both effects by using the forward-folding formalism described in Ref. [15] in the fit of the spectrum. We fitted a spectrum model consisting of a broken power law with soft transitions, the same functional form used for the two other surface-detector spectra,

$$J(E) = J_0 \left(\frac{E}{100\,\mathrm{PeV}}\right)^{\gamma_0} \left[1 + \left(\frac{E}{E_{01}}\right)^{\frac{1}{\omega_{01}}}\right]^{(\gamma_0-\gamma_1)\,\omega_{01}}, \tag{5}$$

where $J_0 = (0.97 \pm 0.02)\times 10^{-13}\,\mathrm{km^{-2}\,sr^{-1}\,eV^{-1}}$ is the normalization parameter, $\lg(E_{01}/\mathrm{eV}) = 17.37 \pm 0.10$ is the energy of the transition, $\gamma_0 = 3.00 \pm 0.05$ is the spectral index before the break, and $\gamma_1 = 3.32 \pm 0.08$ is the spectral index after the break. The width of the transition $\omega_{01} = 0.25$ was fixed in the fit to the value obtained in [5]. We tried to free this parameter but could not constrain it due to our sensitivity. The correction that arises from the unfolding procedure is close to 5% in all the energy range. Fig. 5 shows the spectrum measured with the SD433 after the unfolding correction is applied. We up-scaled the flux by E^3 to highlight the observed break in the spectrum. As it is the case for the SD750, the SD433 energy has a systematic uncertainty of 14% that is almost energy independent. This uncertainty is dominated by the contribution of the uncertainty of the fluorescence detector energy. The uncertainty in the energy corresponds to a $\simeq$35% uncertainty in the flux which leads to a systematic uncertainty of $0.34 \times 10^{-13}\,\mathrm{km^{-2}\,sr^{-1}\,eV^{-1}}$ in the parameter J_0. The corresponding energy of the second knee including the systematic uncertainty that comes from the energy scale is $E_{01} = (230 \pm 50\,\mathrm{stat} \pm 35\,\mathrm{syst})$ PeV. This uncertainty is also propagated to the spectral indexes in the unfolding procedure leading to $\gamma_0 = 3.00 \pm 0.05\,\mathrm{stat} \pm 0.10\,\mathrm{syst}$ and $\gamma_1 = 3.32 \pm 0.08\,\mathrm{stat} \pm 0.10\,\mathrm{syst}$. We are currently working to assess the influence of subdominant sources of systematic uncertainties.

This is the first measurement of all the spectral features of the second knee with an Auger surface detector. Although the SD750 already hinted the second knee [8], it only measured the spectral index after the break given a loss of its efficiency around the energy of the break. At that time, the spectral index after the break was $\gamma = 3.34 \pm 0.02$, which is consistent within statistical uncertainties with the current SD433 measurement. Moreover, the fluxes measured with SD433 and SD750 are within 5% with respect to one another.

Our measurement is also consistent within the uncertainties with a previous report from Auger where the spectrum around the second knee that was obtained by extrapolating the 750 m spectrum below 0.1 EeV using the Cherekov dominated FD events [5]. Fig. 6 shows the SD433 spectrum along with the measurements of other experiments and the previous Auger report.

5. Conclusions

We have presented in this work the cosmic ray spectrum measured with the Auger surface detector spaced at 433 m. This array, denser than the two other Auger ones, lowers the threshold energy reachable with the surface detector to $E = 63$ PeV thus covering the second knee. We are reporting, for the first time, all the second-knee spectral features as seen by the surface detector of the Pierre Auger Observatory. We have located the second knee at $(230 \pm 50\,\mathrm{stat} \pm 35\,\mathrm{syst})$ PeV,

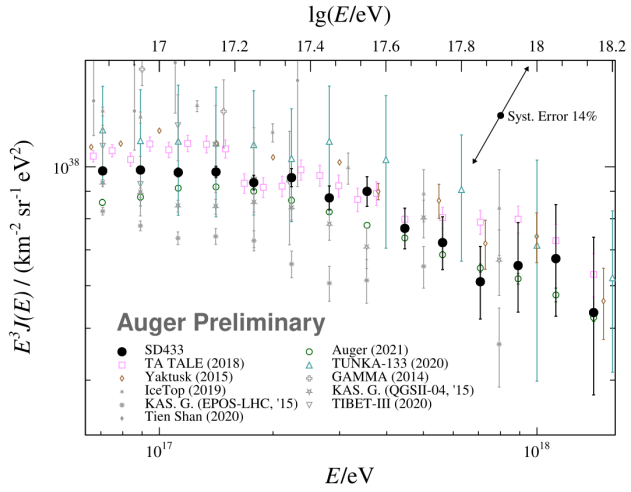

Figure 6: SD433 spectrum scaled by E^3 along with Auger combined measurement [5] and the measurements of other experiments around the second knee (references in [8]). Experiments that set their energy scale calorimetrically are shown in color. The systematic uncertainty of Auger is plotted.

at which point the spectral index increases from $\gamma_0 = 3.00 \pm 0.05\,\text{stat} \pm 0.10\,\text{syst}$ to $\gamma_1 = 3.32 \pm 0.08\,\text{stat} \pm 0.10\,\text{syst}$. The 433 m array has a robust exposure computation, calorimetric calibration in energy, and covers a broad energy region around the second knee, making it possible to fully characterize this feature. A preliminary observation of the second knee has also been reported in [5], using Cherenkov dominated FD events. The final uncertainty estimation of this previous result, as well as the measurement presented here, are yet to be finalized. However, both characterizations of the second knee feature are consistent within preliminary estimates of the systematics.

References

[1] M. Nagano *et al.*, J. Phys. G **18** (1992) 423–442, doi:10.1088/0954-3899/18/2/022.
[2] T. AbuZayyad *et al.* [Telescope Array], **PoS** (ICRC2021) 347, doi:10.22323/1.395.0347.
[3] W.D. Apel *et al.*, Astropart. Phys. **36** (2012) 183–194, doi:10.1016/j.astropartphys.2012.05.023.
[4] N.M. Budnev *et al.*, Astropart. Phys. **117** (2020) 102406, doi:10.1016/j.astropartphys.2019.102406.
[5] V. Novotný [Pierre Auger Coll.], **PoS** (ICRC2021) 324, doi:10.22323/1.395.0324.
[6] J. de Jesús [Pierre Auger Coll.], these proceedings.
[7] N. Gonzalez [Pierre Auger Coll.], these proceedings.
[8] P. Abreu *et al.* [Pierre Auger Coll.], Eur. Phys. J. C **81** (2021) 966, doi:10.1140/epjc/s10052-021-09700-w.
[9] A. Aab *et al.* [Pierre Auger Coll.], Nucl. Instrum. Meth. A **798** (2015) 172–213, doi:10.1016/j.nima.2015.06.058.
[10] H.P. Dembinski *et al.*, **PoS** (ICRC2017) 533, doi:10.22323/1.301.0533.
[11] S. Argiro *et al.*, Nucl. Instrum. Meth. A **580** (2007) 1485–1496, doi:10.1016/j.nima.2007.07.010.
[12] G. Silli [Pierre Auger Coll.], **PoS** (ICRC2021) 224, doi:10.22323/1.395.0224.
[13] H. P. Dembinski *et al.*, Astropart. Phys. **73** (2016), 44-51 doi:10.1016/j.astropartphys.2015.08.001.
[14] J. Abraham *et al.* [Pierre Auger Coll.], Nucl. Instrum. Meth. A **613** (2010) 29–39, doi:10.1016/j.nima.2009.11.018.
[15] A. Aab *et al.* [Pierre Auger Coll.], Phys. Rev. D **102** (2020) 062005, doi:10.1103/PhysRevD.102.062005.

The Pierre Auger Collaboration

A. Abdul Halim[13], P. Abreu[72], M. Aglietta[54,52], I. Allekotte[1], K. Almeida Cheminant[70], A. Almela[7,12], R. Aloisio[45,46], J. Alvarez-Muñiz[79], J. Ammerman Yebra[79], G.A. Anastasi[54,52], L. Anchordoqui[86], B. Andrada[7], S. Andringa[72], C. Aramo[50], P.R. Araújo Ferreira[42], E. Arnone[63,52], J. C. Arteaga Velázquez[67], H. Asorey[7], P. Assis[72], G. Avila[11], E. Avocone[57,46], A.M. Badescu[75], A. Bakalova[32], A. Balaceanu[73], F. Barbato[45,46], A. Bartz Mocellin[85], J.A. Bellido[13,69], C. Berat[36], M.E. Bertaina[63,52], G. Bhatta[70], M. Bianciotto[63,52], P.L. Biermann[h], V. Binet[5], K. Bismark[39,7], T. Bister[80,81], J. Biteau[37], J. Blazek[32], C. Bleve[36], J. Blümer[41], M. Boháčová[32], D. Boncioli[57,46], C. Bonifazi[8,26], L. Bonneau Arbeletche[21], N. Borodai[70], J. Brack[j], P.G. Brichetto Orchera[7], F.L. Briechle[42], A. Bueno[78], S. Buitink[15], M. Buscemi[47,61], M. Büsken[39,7], A. Bwembya[80,81], K.S. Caballero-Mora[66], S. Cabana-Freire[79], L. Caccianiga[59,49], I. Caracas[38], R. Caruso[58,47], A. Castellina[54,52], F. Catalani[18], G. Cataldi[48], L. Cazon[79], M. Cerda[10], A. Cermenati[45,46], J.A. Chinellato[21], J. Chudoba[32], L. Chytka[33], R.W. Clay[13], A.C. Cobos Cerutti[6], R. Colalillo[60,50], A. Coleman[90], M.R. Coluccia[48], R. Conceição[72], A. Condorelli[37], G. Consolati[49,55], M. Conte[56,48], F. Convenga[41], D. Correia dos Santos[28], P.J. Costa[72], C.E. Covault[84], M. Cristinziani[44], C.S. Cruz Sanchez[3], S. Dasso[4,2], K. Daumiller[41], B.R. Dawson[13], R.M. de Almeida[28], J. de Jesús[7,41], S.J. de Jong[80,81], J.R.T. de Mello Neto[26,27], I. De Mitri[45,46], J. de Oliveira[17], D. de Oliveira Franco[21], F. de Palma[56,48], V. de Souza[19], E. De Vito[56,48], A. Del Popolo[58,47], O. Deligny[34], N. Denner[32], L. Deval[41,7], A. di Matteo[52], M. Dobre[73], C. Dobrigkeit[21], J.C. D'Olivo[68], L.M. Domingues Mendes[72], J.C. dos Anjos, R.C. dos Anjos[25], J. Ebr[32], F. Ellwanger[41], M. Emam[80,81], R. Engel[39,41], I. Epicoco[56,48], M. Erdmann[42], A. Etchegoyen[7,12], C. Evoli[45,46], H. Falcke[80,82,81], J. Farmer[89], G. Farrar[88], A.C. Fauth[21], N. Fazzini[e], F. Feldbusch[40], F. Fenu[41,d], A. Fernandes[72], B. Fick[87], J.M. Figueira[7], A. Filipčič[77,76], T. Fitoussi[41], B. Flaggs[90], T. Fodran[80], T. Fujii[89,f], A. Fuster[7,12], C. Galea[80], C. Galelli[59,49], B. García[6], C. Gaudu[38], H. Gemmeke[40], F. Gesualdi[7,41], A. Gherghel-Lascu[73], P.L. Ghia[34], U. Giaccari[48], M. Giammarchi[49], J. Glombitza[42,g], F. Gobbi[10], F. Gollan[7], G. Golup[1], M. Gómez Berisso[1], P.F. Gómez Vitale[11], J.P. Gongora[11], J.M. González[1], N. González[7], I. Goos[1], D. Góra[70], A. Gorgi[54,52], M. Gottowik[79], T.D. Grubb[13], F. Guarino[60,50], G.P. Guedes[22], E. Guido[44], S. Hahn[39], P. Hamal[32], M.R. Hampel[7], P. Hansen[3], D. Harari[1], V.M. Harvey[13], A. Haungs[41], T. Hebbeker[42], C. Hojvat[e], J.R. Hörandel[80,81], P. Horvath[33], M. Hrabovský[33], T. Huege[41,15], A. Insolia[58,47], P.G. Isar[74], P. Janecek[32], J.A. Johnsen[85], J. Jurysek[32], A. Kääpä[38], K.H. Kampert[38], B. Keilhauer[41], A. Khakurdikar[80], V.V. Kizakke Covilakam[7,41], H.O. Klages[41], M. Kleifges[40], F. Knapp[39], N. Kunka[40], B.L. Lago[16], N. Langner[42], M.A. Leigui de Oliveira[24], Y Lema-Capeans[79], V. Lenok[39], A. Letessier-Selvon[35], I. Lhenry-Yvon[34], D. Lo Presti[58,47], L. Lopes[72], L. Lu[91], Q. Luce[39], J.P. Lundquist[76], A. Machado Payeras[21], M. Majercakova[32], D. Mandat[32], B.C. Manning[13], P. Mantsch[e], S. Marafico[34], F.M. Mariani[59,49], A.G. Mariazzi[3], I.C. Mariş[14], G. Marsella[61,47], D. Martello[56,48], S. Martinelli[41,7], O. Martínez Bravo[64], M.A. Martins[79], M. Mastrodicasa[57,46], H.J. Mathes[41], J. Matthews[a], G. Matthiae[62,51], E. Mayotte[85,38], S. Mayotte[85], P.O. Mazur[e], G. Medina-Tanco[68], J. Meinert[38], D. Melo[7], A. Menshikov[40], C. Merx[41], S. Michal[33], M.I. Micheletti[5], L. Miramonti[59,49], S. Mollerach[1], F. Montanet[36], L. Morejon[38], C. Morello[54,52], A.L. Müller[32], K. Mulrey[80,81], R. Mussa[52], M. Muzio[88], W.M. Namasaka[38], S. Negi[32], L. Nellen[68], K. Nguyen[87], G. Nicora[9], M. Niculescu-Oglinzanu[73], M. Niechciol[44], D. Nitz[87], D. Nosek[31], V. Novotny[31], L. Nožka[33], A Nucita[56,48], L.A. Núñez[30], C. Oliveira[19], M. Palatka[32], J. Pallotta[9], S. Panja[32], G. Parente[79], T. Paulsen[38], J. Pawlowsky[38], M. Pech[32], J. Pękala[70], R. Pelayo[65], L.A.S. Pereira[23], E.E. Pereira Martins[39,7], J. Perez Armand[20], C. Pérez Bertolli[7,41], L. Perrone[56,48], S. Petrera[45,46], C. Petrucci[57,46], T. Pierog[41], M. Pimenta[72], M. Platino[7], B. Pont[80], M. Pothast[81,80], M. Pourmohammad Shahvar[61,47], P. Privitera[89], M. Prouza[32], A. Puyleart[87], S. Querchfeld[38], J. Rautenberg[38], D. Ravignani[7], M. Reininghaus[39], J. Ridky[32], F. Riehn[79], M. Risse[44], V. Rizi[57,46], W. Rodrigues de Carvalho[80], E. Rodriguez[7,41], J. Rodriguez Rojo[11], M.J. Roncoroni[7], S. Rossoni[43], M. Roth[41], E. Roulet[1], A.C. Rovero[4], P. Ruehl[44], A. Saftoiu[73], M. Saharan[80], F. Salamida[57,46], H. Salazar[64], G. Salina[51], J.D. Sanabria Gomez[30], F. Sánchez[7], E.M. Santos[20], E. Santos[32],

F. Sarazin[85], R. Sarmento[72], R. Sato[11], P. Savina[91], C.M. Schäfer[41], V. Scherini[56,48], H. Schieler[41], M. Schimassek[34], M. Schimp[38], F. Schlüter[41], D. Schmidt[39], O. Scholten[15,i], H. Schoorlemmer[80,81], P. Schovánek[32], F.G. Schröder[90,41], J. Schulte[42], T. Schulz[41], S.J. Sciutto[3], M. Scornavacche[7,41], A. Segreto[53,47], S. Sehgal[38], S.U. Shivashankara[76], G. Sigl[43], G. Silli[7], O. Sima[73,b], F. Simon[40], R. Smau[73], R. Šmída[89], P. Sommers[k], J.F. Soriano[86], R. Squartini[10], M. Stadelmaier[32], D. Stanca[73], S. Stanič[76], J. Stasielak[70], P. Stassi[36], S. Strähnz[39], M. Straub[42], M. Suárez-Durán[14], T. Suomijärvi[37], A.D. Supanitsky[7], Z. Svozilikova[32], Z. Szadkowski[71], A. Tapia[29], C. Taricco[63,52], C. Timmermans[81,80], O. Tkachenko[41], P. Tobiska[32], C.J. Todero Peixoto[18], B. Tomé[72], Z. Torrès[36], A. Travaini[10], P. Travnicek[32], C. Trimarelli[57,46], M. Tueros[3], M. Unger[41], L. Vaclavek[33], M. Vacula[33], J.F. Valdés Galicia[68], L. Valore[60,50], E. Varela[64], A. Vásquez-Ramírez[30], D. Veberič[41], C. Ventura[27], I.D. Vergara Quispe[3], V. Verzi[51], J. Vicha[32], J. Vink[83], J. Vlastimil[32], S. Vorobiov[76], C. Watanabe[26], A.A. Watson[c], A. Weindl[41], L. Wiencke[85], H. Wilczyński[70], D. Wittkowski[38], B. Wundheiler[7], B. Yue[38], A. Yushkov[32], O. Zapparrata[14], E. Zas[79], D. Zavrtanik[76,77], M. Zavrtanik[77,76]

———— • ————

[1] Centro Atómico Bariloche and Instituto Balseiro (CNEA-UNCuyo-CONICET), San Carlos de Bariloche, Argentina
[2] Departamento de Física and Departamento de Ciencias de la Atmósfera y los Océanos, FCEyN, Universidad de Buenos Aires and CONICET, Buenos Aires, Argentina
[3] IFLP, Universidad Nacional de La Plata and CONICET, La Plata, Argentina
[4] Instituto de Astronomía y Física del Espacio (IAFE, CONICET-UBA), Buenos Aires, Argentina
[5] Instituto de Física de Rosario (IFIR) – CONICET/U.N.R. and Facultad de Ciencias Bioquímicas y Farmacéuticas U.N.R., Rosario, Argentina
[6] Instituto de Tecnologías en Detección y Astropartículas (CNEA, CONICET, UNSAM), and Universidad Tecnológica Nacional – Facultad Regional Mendoza (CONICET/CNEA), Mendoza, Argentina
[7] Instituto de Tecnologías en Detección y Astropartículas (CNEA, CONICET, UNSAM), Buenos Aires, Argentina
[8] International Center of Advanced Studies and Instituto de Ciencias Físicas, ECyT-UNSAM and CONICET, Campus Miguelete – San Martín, Buenos Aires, Argentina
[9] Laboratorio Atmósfera – Departamento de Investigaciones en Láseres y sus Aplicaciones – UNIDEF (CITEDEF-CONICET), Argentina
[10] Observatorio Pierre Auger, Malargüe, Argentina
[11] Observatorio Pierre Auger and Comisión Nacional de Energía Atómica, Malargüe, Argentina
[12] Universidad Tecnológica Nacional – Facultad Regional Buenos Aires, Buenos Aires, Argentina
[13] University of Adelaide, Adelaide, S.A., Australia
[14] Université Libre de Bruxelles (ULB), Brussels, Belgium
[15] Vrije Universiteit Brussels, Brussels, Belgium
[16] Centro Federal de Educação Tecnológica Celso Suckow da Fonseca, Petropolis, Brazil
[17] Instituto Federal de Educação, Ciência e Tecnologia do Rio de Janeiro (IFRJ), Brazil
[18] Universidade de São Paulo, Escola de Engenharia de Lorena, Lorena, SP, Brazil
[19] Universidade de São Paulo, Instituto de Física de São Carlos, São Carlos, SP, Brazil
[20] Universidade de São Paulo, Instituto de Física, São Paulo, SP, Brazil
[21] Universidade Estadual de Campinas, IFGW, Campinas, SP, Brazil
[22] Universidade Estadual de Feira de Santana, Feira de Santana, Brazil
[23] Universidade Federal de Campina Grande, Centro de Ciencias e Tecnologia, Campina Grande, Brazil
[24] Universidade Federal do ABC, Santo André, SP, Brazil
[25] Universidade Federal do Paraná, Setor Palotina, Palotina, Brazil
[26] Universidade Federal do Rio de Janeiro, Instituto de Física, Rio de Janeiro, RJ, Brazil
[27] Universidade Federal do Rio de Janeiro (UFRJ), Observatório do Valongo, Rio de Janeiro, RJ, Brazil
[28] Universidade Federal Fluminense, EEIMVR, Volta Redonda, RJ, Brazil
[29] Universidad de Medellín, Medellín, Colombia
[30] Universidad Industrial de Santander, Bucaramanga, Colombia

[31] Charles University, Faculty of Mathematics and Physics, Institute of Particle and Nuclear Physics, Prague, Czech Republic
[32] Institute of Physics of the Czech Academy of Sciences, Prague, Czech Republic
[33] Palacky University, Olomouc, Czech Republic
[34] CNRS/IN2P3, IJCLab, Université Paris-Saclay, Orsay, France
[35] Laboratoire de Physique Nucléaire et de Hautes Energies (LPNHE), Sorbonne Université, Université de Paris, CNRS-IN2P3, Paris, France
[36] Univ. Grenoble Alpes, CNRS, Grenoble Institute of Engineering Univ. Grenoble Alpes, LPSC-IN2P3, 38000 Grenoble, France
[37] Université Paris-Saclay, CNRS/IN2P3, IJCLab, Orsay, France
[38] Bergische Universität Wuppertal, Department of Physics, Wuppertal, Germany
[39] Karlsruhe Institute of Technology (KIT), Institute for Experimental Particle Physics, Karlsruhe, Germany
[40] Karlsruhe Institute of Technology (KIT), Institut für Prozessdatenverarbeitung und Elektronik, Karlsruhe, Germany
[41] Karlsruhe Institute of Technology (KIT), Institute for Astroparticle Physics, Karlsruhe, Germany
[42] RWTH Aachen University, III. Physikalisches Institut A, Aachen, Germany
[43] Universität Hamburg, II. Institut für Theoretische Physik, Hamburg, Germany
[44] Universität Siegen, Department Physik – Experimentelle Teilchenphysik, Siegen, Germany
[45] Gran Sasso Science Institute, L'Aquila, Italy
[46] INFN Laboratori Nazionali del Gran Sasso, Assergi (L'Aquila), Italy
[47] INFN, Sezione di Catania, Catania, Italy
[48] INFN, Sezione di Lecce, Lecce, Italy
[49] INFN, Sezione di Milano, Milano, Italy
[50] INFN, Sezione di Napoli, Napoli, Italy
[51] INFN, Sezione di Roma "Tor Vergata", Roma, Italy
[52] INFN, Sezione di Torino, Torino, Italy
[53] Istituto di Astrofisica Spaziale e Fisica Cosmica di Palermo (INAF), Palermo, Italy
[54] Osservatorio Astrofisico di Torino (INAF), Torino, Italy
[55] Politecnico di Milano, Dipartimento di Scienze e Tecnologie Aerospaziali , Milano, Italy
[56] Università del Salento, Dipartimento di Matematica e Fisica "E. De Giorgi", Lecce, Italy
[57] Università dell'Aquila, Dipartimento di Scienze Fisiche e Chimiche, L'Aquila, Italy
[58] Università di Catania, Dipartimento di Fisica e Astronomia "Ettore Majorana", Catania, Italy
[59] Università di Milano, Dipartimento di Fisica, Milano, Italy
[60] Università di Napoli "Federico II", Dipartimento di Fisica "Ettore Pancini", Napoli, Italy
[61] Università di Palermo, Dipartimento di Fisica e Chimica "E. Segrè", Palermo, Italy
[62] Università di Roma "Tor Vergata", Dipartimento di Fisica, Roma, Italy
[63] Università Torino, Dipartimento di Fisica, Torino, Italy
[64] Benemérita Universidad Autónoma de Puebla, Puebla, México
[65] Unidad Profesional Interdisciplinaria en Ingeniería y Tecnologías Avanzadas del Instituto Politécnico Nacional (UPIITA-IPN), México, D.F., México
[66] Universidad Autónoma de Chiapas, Tuxtla Gutiérrez, Chiapas, México
[67] Universidad Michoacana de San Nicolás de Hidalgo, Morelia, Michoacán, México
[68] Universidad Nacional Autónoma de México, México, D.F., México
[69] Universidad Nacional de San Agustin de Arequipa, Facultad de Ciencias Naturales y Formales, Arequipa, Peru
[70] Institute of Nuclear Physics PAN, Krakow, Poland
[71] University of Łódź, Faculty of High-Energy Astrophysics,Łódź, Poland
[72] Laboratório de Instrumentação e Física Experimental de Partículas – LIP and Instituto Superior Técnico – IST, Universidade de Lisboa – UL, Lisboa, Portugal
[73] "Horia Hulubei" National Institute for Physics and Nuclear Engineering, Bucharest-Magurele, Romania
[74] Institute of Space Science, Bucharest-Magurele, Romania
[75] University Politehnica of Bucharest, Bucharest, Romania
[76] Center for Astrophysics and Cosmology (CAC), University of Nova Gorica, Nova Gorica, Slovenia
[77] Experimental Particle Physics Department, J. Stefan Institute, Ljubljana, Slovenia

PoS(ICRC2023)398

[78] Universidad de Granada and C.A.F.P.E., Granada, Spain
[79] Instituto Galego de Física de Altas Enerxías (IGFAE), Universidade de Santiago de Compostela, Santiago de Compostela, Spain
[80] IMAPP, Radboud University Nijmegen, Nijmegen, The Netherlands
[81] Nationaal Instituut voor Kernfysica en Hoge Energie Fysica (NIKHEF), Science Park, Amsterdam, The Netherlands
[82] Stichting Astronomisch Onderzoek in Nederland (ASTRON), Dwingeloo, The Netherlands
[83] Universiteit van Amsterdam, Faculty of Science, Amsterdam, The Netherlands
[84] Case Western Reserve University, Cleveland, OH, USA
[85] Colorado School of Mines, Golden, CO, USA
[86] Department of Physics and Astronomy, Lehman College, City University of New York, Bronx, NY, USA
[87] Michigan Technological University, Houghton, MI, USA
[88] New York University, New York, NY, USA
[89] University of Chicago, Enrico Fermi Institute, Chicago, IL, USA
[90] University of Delaware, Department of Physics and Astronomy, Bartol Research Institute, Newark, DE, USA
[91] University of Wisconsin-Madison, Department of Physics and WIPAC, Madison, WI, USA

—

[a] Louisiana State University, Baton Rouge, LA, USA
[b] also at University of Bucharest, Physics Department, Bucharest, Romania
[c] School of Physics and Astronomy, University of Leeds, Leeds, United Kingdom
[d] now at Agenzia Spaziale Italiana (ASI). Via del Politecnico 00133, Roma, Italy
[e] Fermi National Accelerator Laboratory, Fermilab, Batavia, IL, USA
[f] now at Graduate School of Science, Osaka Metropolitan University, Osaka, Japan
[g] now at ECAP, Erlangen, Germany
[h] Max-Planck-Institut für Radioastronomie, Bonn, Germany
[i] also at Kapteyn Institute, University of Groningen, Groningen, The Netherlands
[j] Colorado State University, Fort Collins, CO, USA
[k] Pennsylvania State University, University Park, PA, USA

Acknowledgments

The successful installation, commissioning, and operation of the Pierre Auger Observatory would not have been possible without the strong commitment and effort from the technical and administrative staff in Malargüe. We are very grateful to the following agencies and organizations for financial support:

Argentina – Comisión Nacional de Energía Atómica; Agencia Nacional de Promoción Científica y Tecnológica (ANPCyT); Consejo Nacional de Investigaciones Científicas y Técnicas (CONICET); Gobierno de la Provincia de Mendoza; Municipalidad de Malargüe; NDM Holdings and Valle Las Leñas; in gratitude for their continuing cooperation over land access; Australia – the Australian Research Council; Belgium – Fonds de la Recherche Scientifique (FNRS); Research Foundation Flanders (FWO); Brazil – Conselho Nacional de Desenvolvimento Científico e Tecnológico (CNPq); Financiadora de Estudos e Projetos (FINEP); Fundação de Amparo à Pesquisa do Estado de Rio de Janeiro (FAPERJ); São Paulo Research Foundation (FAPESP) Grants No. 2019/10151-2, No. 2010/07359-6 and No. 1999/05404-3; Ministério da Ciência, Tecnologia, Inovações e Comunicações (MCTIC); Czech Republic – Grant No. MSMT CR LTT18004, LM2015038, LM2018102, CZ.02.1.01/0.0/0.0/16_013/0001402, CZ.02.1.01/0.0/0.0/18_046/0016010 and CZ.02.1.01/0.0/0.0/17_049/0008422; France – Centre de Calcul IN2P3/CNRS; Centre National de la Recherche Scientifique (CNRS); Conseil Régional Ile-de-France; Département Physique Nucléaire et Corpusculaire (PNC-IN2P3/CNRS); Département Sciences de l'Univers (SDU-INSU/CNRS); Institut Lagrange de Paris (ILP) Grant No. LABEX ANR-10-LABX-63 within the Investissements d'Avenir Programme Grant No. ANR-11-IDEX-0004-02; Germany – Bundesministerium für Bildung und Forschung (BMBF); Deutsche Forschungsgemeinschaft (DFG); Finanzministerium Baden-Württemberg; Helmholtz Alliance for Astroparticle Physics (HAP); Helmholtz-Gemeinschaft Deutscher Forschungszentren (HGF); Ministerium für Kultur und Wissenschaft des Landes Nordrhein-Westfalen; Ministerium für Wissenschaft, Forschung und Kunst des Landes Baden-Württemberg; Italy – Istituto Nazionale di Fisica Nucleare (INFN); Istituto Nazionale di Astrofisica (INAF); Ministero dell'Universitá e della Ricerca (MIUR); CETEMPS Center of Excellence; Ministero degli Affari Esteri (MAE), ICSC Centro Nazionale di Ricerca in High Performance Computing, Big Data

and Quantum Computing, funded by European Union NextGenerationEU, reference code CN_00000013; México – Consejo Nacional de Ciencia y Tecnología (CONACYT) No. 167733; Universidad Nacional Autónoma de México (UNAM); PAPIIT DGAPA-UNAM; The Netherlands – Ministry of Education, Culture and Science; Netherlands Organisation for Scientific Research (NWO); Dutch national e-infrastructure with the support of SURF Cooperative; Poland – Ministry of Education and Science, grants No. DIR/WK/2018/11 and 2022/WK/12; National Science Centre, grants No. 2016/22/M/ST9/00198, 2016/23/B/ST9/01635, 2020/39/B/ST9/01398, and 2022/45/B/ST9/02163; Portugal – Portuguese national funds and FEDER funds within Programa Operacional Factores de Competitividade through Fundação para a Ciência e a Tecnologia (COMPETE); Romania – Ministry of Research, Innovation and Digitization, CNCS-UEFISCDI, contract no. 30N/2023 under Romanian National Core Program LAPLAS VII, grant no. PN 23 21 01 02 and project number PN-III-P1-1.1-TE-2021-0924/TE57/2022, within PNCDI III; Slovenia – Slovenian Research Agency, grants P1-0031, P1-0385, I0-0033, N1-0111; Spain – Ministerio de Economía, Industria y Competitividad (FPA2017-85114-P and PID2019-104676GB-C32), Xunta de Galicia (ED431C 2017/07), Junta de Andalucía (SOMM17/6104/UGR, P18-FR-4314) Feder Funds, RENATA Red Nacional Temática de Astropartículas (FPA2015-68783-REDT) and María de Maeztu Unit of Excellence (MDM-2016-0692); USA – Department of Energy, Contracts No. DE-AC02-07CH11359, No. DE-FR02-04ER41300, No. DE-FG02-99ER41107 and No. DE-SC0011689; National Science Foundation, Grant No. 0450696; The Grainger Foundation; Marie Curie-IRSES/EPLANET; European Particle Physics Latin American Network; and UNESCO.